Electronic Supplementary Material (ESI) for Journal of Materials Chemistry A.
This journal is © The Royal Society of Chemistry 2024

Supplementary Information

Enhancing Performance and Cyclability of MoS_2 Cathodes with Interspace layer Engineering using Polypyrrole

Nima Mikaeili Chahartagh[a], Ali Molaei Aghdam *[a,b] , Shahriar Namvar[c], and Mehryar Jafari[d]

[a] *Department of Chemical Engineering, Amirkabir University of Technology (Tehran Polytechnic), PO Box 15875-4413, Tehran, Iran*

[b]*Department of Chemical Engineering, Auburn University, Auburn, AL 36849, United States*

[c]*Department of Mechanical and Industrial Engineering, University of Illinois at Chicago, Chicago, IL, 60607 USA*

[d] *Chemical engineering department, University of Bath, Claverton Down, Bath BA2 7AY, UK.*

E-mail: azm0382@auburn.edu

Materials Characterizations

On an X-ray diffractometer (Bruker D2 Phaser), the sample crystal structures were examined using copper-Kα radiation (λ = 1.54178 Å) throughout a 2θ range of 5 to 80 degrees. SEM (Philips XL 30) and TEM (Philips EM208) were used to examine the microstructure and morphology of the samples. A spectrometer (BRUKER-ALPHA) gathered Fourier transform infrared (FTIR) spectra. XPS measurements (PHI 5500) were taken to analyze the surface elemental composition and the corresponding valance states. HRTEM was performed using a field emission electron microscope (JEM-3000F (JEOL)) operating at 300 kV. EDX elemental mapping and HAADF-STEM investigations were done on a JEOL JEM-ARM200CF at 200 kV. A probe aberration corrector was installed in a STEM.

Electrochemical Measurements

The dispersion of PVDF (10 wt%) binder, super black carbon (20 wt%), and active materials (70 wt%) were performed in N-Methyl pyrrolidone. The resultant slurry was cast onto Carbon cloth to make the working electrode. The electrode was then sliced into circular slices (diameter = 11 mm) with an active mass loading of 1.75-2.1 mg cm^{-2} followed by vacuum drying at 80 °C for 10 hours. Fiber glass separator, working electrode, 3 M $Zn(CF_3SO_3)_2$ aqueous electrolyte, and zinc anode manufactured CR2032 coin cells in ambient air. Between the zinc anode and PPy-MoS_2, the separator was used to complete the AZIB. Charge-discharge cycle measurements were conducted using a Kimiastat battery test system within a voltage range from 0.2 to 1.3 V vs. Zn^{2+}/Zn. CV and electrochemical impedance spectroscopy (EIS) tests were recorded by Autolab (PGSTAT 302 N).

Materials Synthesis

Synthesis of MoS_2: Using a slightly modified version of the typical hydrothermal technique, MoS_2 was prepared. Initially, after dissolving 0.242 g (1 mmol) sodium molybdate (Na2MoO4, AR), 0.05 g (0.14 mmol) cetyltrimethylammonium bromide (CTAB, AR), and 0.151 g (2 mmol) thiocetamide (TAA, AR) in a DI water volume of 20 mL, the solution was subjected to magnetic stirring for ten minutes so as to achieve a uniform solution after complete dissolution. After transferring the same homogenous solution to a polytetrafluoroethylene autoclave (volume of 50 mL), it was maintained at a constant temperature for a period of 24 hours, after which the autoclave was allowed to cool down to the temperature room. Using absolute ethanol and deionized water, the obtained product was rinsed three times. The acquired products (at 200 °C) are labeled as 200-MoS_2 for the purpose of convenience. After drying them for a period of 12 h at a temperature of 60 °C within an oven, the products were characterized further and utilized as the materials of battery cathode.

Synthesis of PPy-MoS_2: Through polymerization, the synthesis of PPy-MoS_2 was conducted. Typically, two grams of powdered MoS_2 undergoes dispersion within DI water (volume of 100 mL). The resulting mixture underwent ultrasonication for a period of 30 minutes so as to disperse the powder evenly. Then, a mixture containing anhydrous ferric chloride and pyrrole monomer (molar ratio of 3:2) was added to the same dispersion. The resulting mixture underwent stirring over an ice bath for a period of 10 hours. Then, the powder of as-synthesized PPy-MoS_2 was dried at a temperature of 80 ◦C.

Zn-ions diffusion coefficient calculation based on the GITT measurement:

The kinetics of Zn^{2+} intercalation during the charge/discharge reaction of PPy-MoS_2 cathode material in depth was investigated using the galvanostatic intermittent titration technique (GITT). The diffusion coefficient of Zn^{2+} (D_{Zn}) was calculated using the following equation:

$$D_{Zn} = \frac{4}{\pi\tau}\left(\frac{mV_m}{MA}\right)^2\left(\frac{\Delta E_s}{\Delta E_\tau}\right)^2$$

Where τ, M, m, V_m, A severally represented the relaxation time, the molar mass of active material, the mass of active material, the molar volume, and the contact area between electrode and electrolyte, while ΔEs and ΔEτ represented the values of pulse voltage change and voltage change of constant-current charge/discharge, respectively.

Computional Details: By employing the Vienna ab initio simulation package (VASP), first-principles computations were carried out on the basis of the density functional theory (DFT) in order to investigate the migration behavior of Zn ions within the PPy-MoS_2 framework[1]. The projector augmented wave (PAW) technique, along with the Perdew–Burke–Ernzerhof (PBE) functional, was employed in the calculations of the electronic structure. In structural optimization, the adopted k-point separation and cut-off energy were 0.00 Å and 500 eV, respectively. In the course of the relaxation, the decided convergence tolerances for energy and force were 10^{-5} eV and 0.01 eV $Å^{-1}$, respectively. In accordance with the spacing between the C atom center within the PPy and the center of the molybdenum atom within the MoS_2 layer, the MoS_2-to-PPy distance

was determined and simulated. By employing the climbing-image nudged elastic band (cNEB) technique, the energy barriers and migration paths could be simulated [2,3].

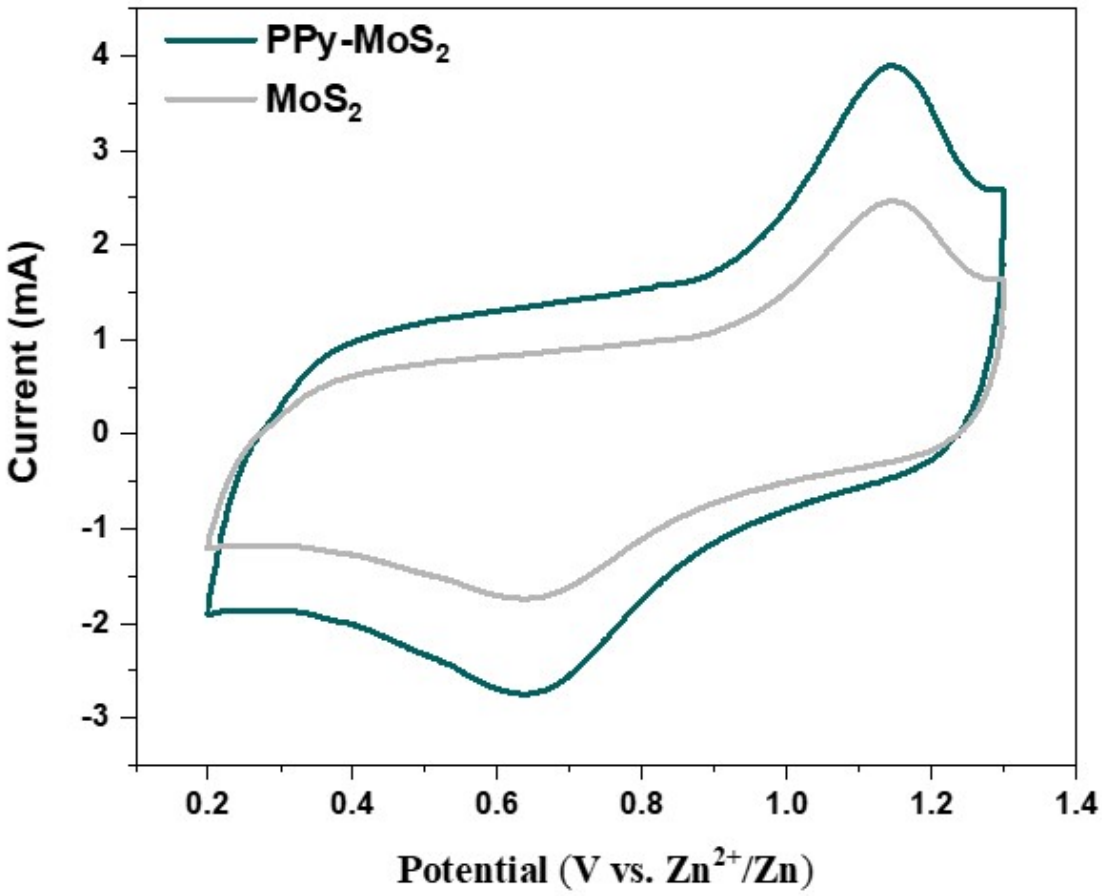

Figure S1. CV curves of MoS_2 cathodes at a scan rate of 0.3 mV s^{-1}.

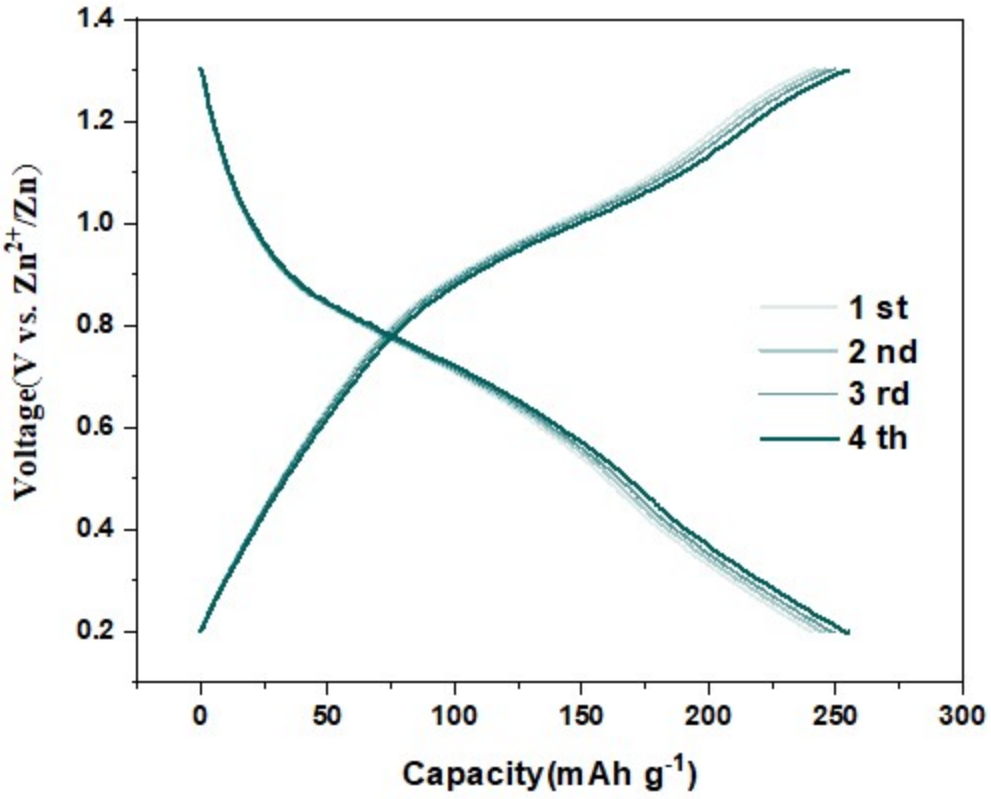

Figure S2. charge/discharge curves at 0.1 A g^{-1} over the voltage range of 0.2-1.3 V of the MoS_2 cathode.

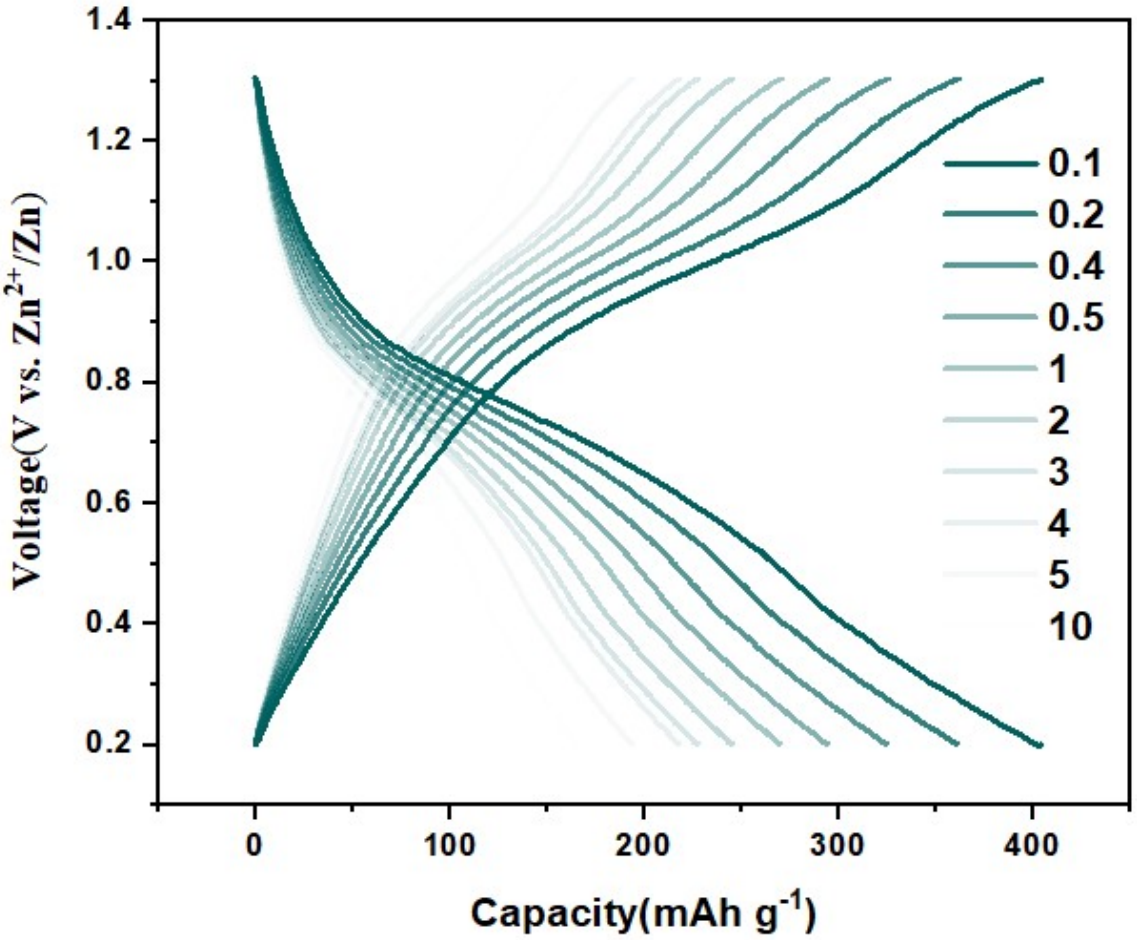

Figure S3. Typical galvanostatic charge and discharge profiles of PPy-MoS_2 cathode for different current densities.

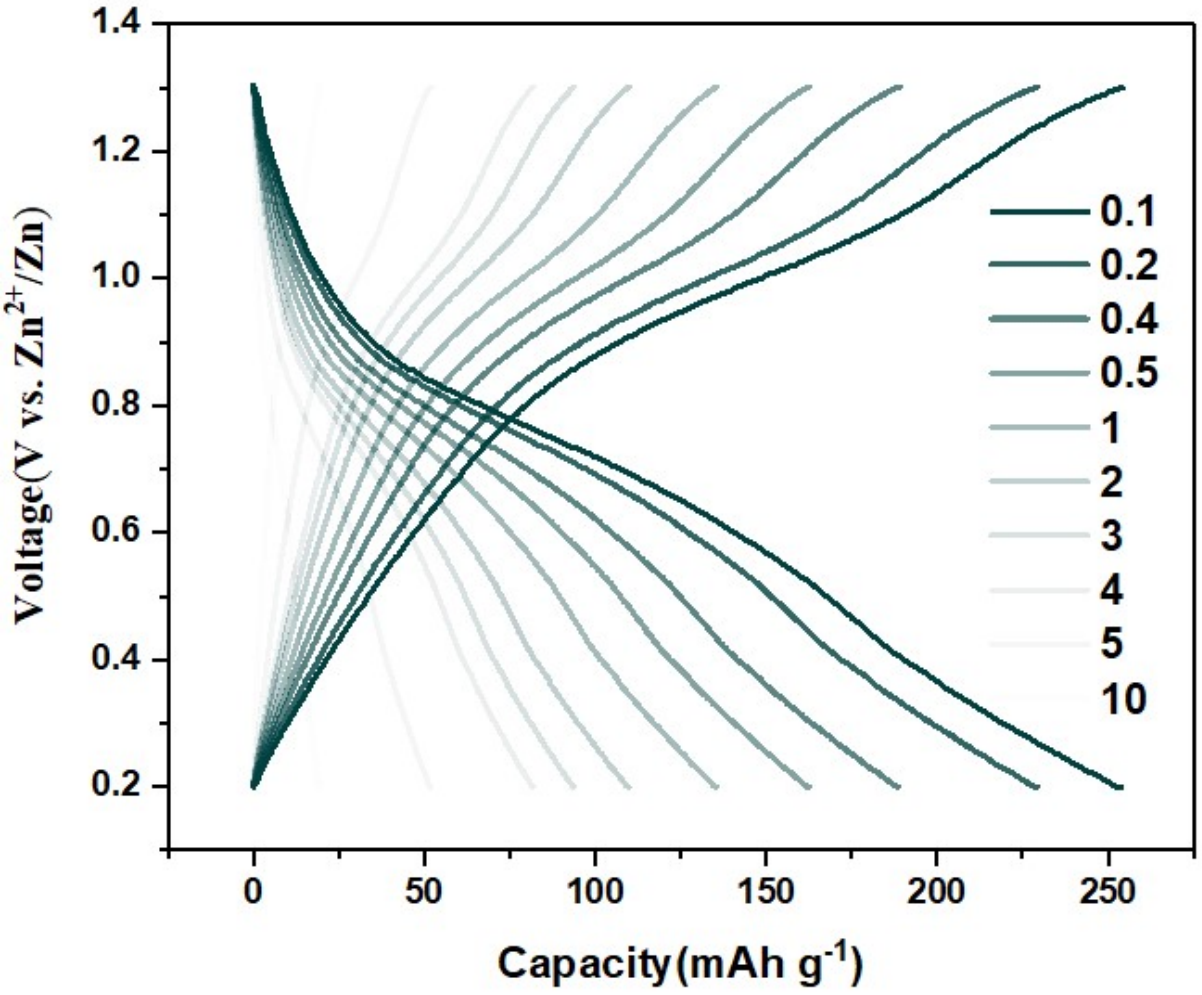

Figure S4. Typical galvanostatic charge and discharge profiles of MoS_2 cathode for different current densities.

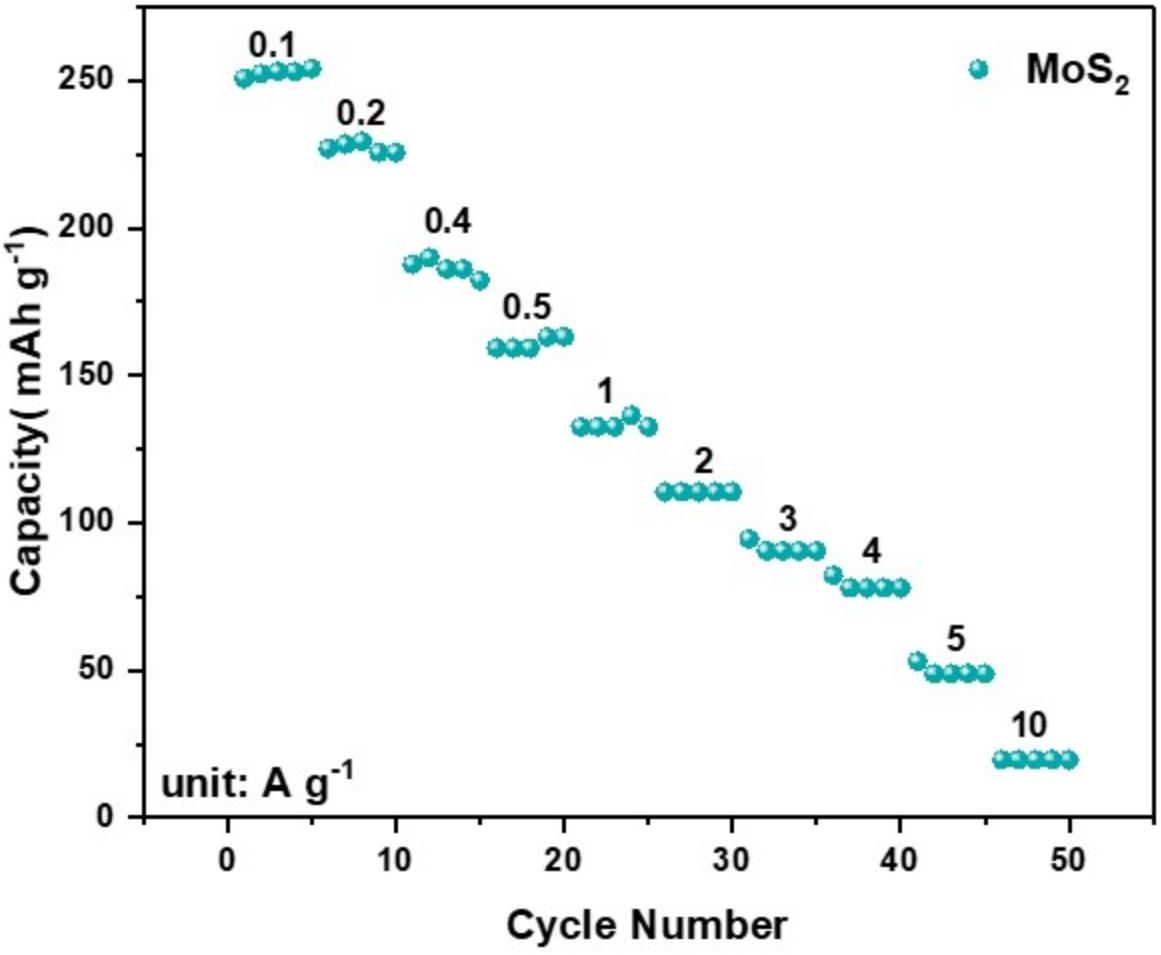

Figure S5. Rate capability at 0.1-10 A g^{-1} of MoS_2 cathode

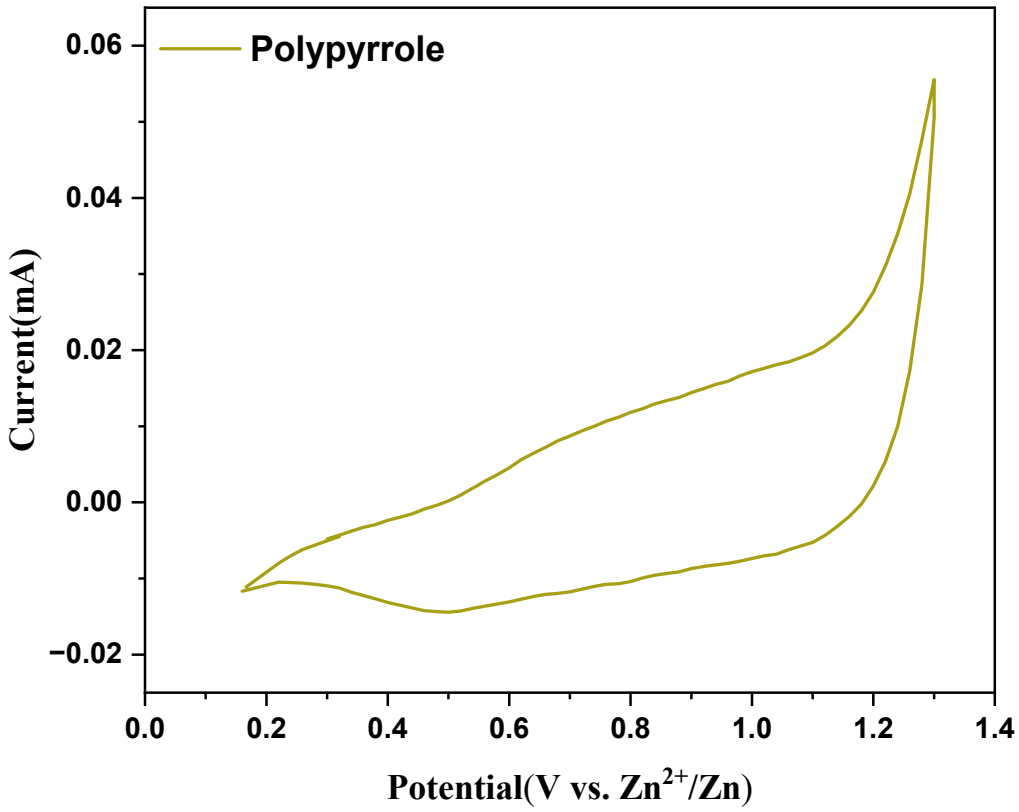

Figure S6. CV curves of PPy at 0.3 mV s^{-1};

Table S1. Summary of the electrochemical properties of transition-metal sulfides and selenides cathodes

Cathode materials	Electrolyte	Voltage	Capacity [mAh g^{-1}]	Cycle stability	Ref
PPy-MoS_2	3 m $Zn(CF_3SO_3)_2$	0.2-1.3 V	404 mAh g^{-1}	83% after 1000 cycles at 5 A g^{-1}	This work
MoS_2/PANI	3 m $Zn(CF_3SO_3)_2$	0.2–1.3 V	106.5 at 1.0 A g^{-1}	86% after 1000 cycles at 1.0 A g^{-1}	4
MoS_2@CF	3 m $Zn(CF_3SO_3)_2$	0.2–1.3 V	182 at 0.1 A g^{-1}	94% over 1500 cycles at 2 A g^{-1}	5
MoS_2-nH_2O	3 m $Zn(CF_3SO_3)_2$	0.2–1.25 V	165 at 0.1 A g^{-1}	88% over 800 cycles at 1 A g^{-1}	6
1T MoS_2	3 m $Zn(CF3SO3)_2$	0.25–1.25 V	165 at 0.1 A g^{-1}	98.1% over 400 cycles at 1 A g^{-1}	7
200-MoS2	3 m $Zn(CF_3SO3)_2$	0.25–1.3 V	148 at 0.5 A g^{-1}	100% after 500 cycles at 2 A g^{-1}	8
Vertical 1T-MoS_2	3 m $Zn(CF_3SO_3)_2$	0.25–1.25 V	198 at 0.1 A g^{-1}	87.8% after 2000 cycles at 1 A g^{-1}	9
1T VS_2	1 m $ZnSO_4$	0.4–1.0 V	190 at 0.01 A g^{-1}	98% after 200 cycles at 0.5 A g^{-1}	10
VS_2@SS	1 m $ZnSO_4$	0.4–1.0 V	190 at 0.05 A g^{-1}	80% after 2000 cycles at 2 A g^{-1}	11
1T WS_2	1 m $ZnSO_4$	0.1–1.5 V	233.26 at 0.05 A g^{-1}	/	12
$TiSe_2$	2 m $ZnSO_4$	0.05–0.6 V	128 at 0.2 A g^{-1}	70% after 300 cycles at 1.0 A g^{-1}	13
VSe_{2-x}-SS	3 m $Zn(CF_3SO_3)_2$	0.4–1.6 V	265.2 at 0.2 A g^{-1}	87.8% over 1800 cycles at 4 A g^{-1}	14
D-MoS_2-O	3 m $Zn(CF_3SO_3)_2$	0.2–1.25 V	261 at 0.1 A g^{-1}	90.5% after 1000 cycles at 1 A g^{-1}	15
Sn vacancy $Co_3Sn_{1.8}S_2$	1 m $Zn(TFSI)_2$	0.01–2.3 V	346 at 0.2 A g^{-1}	83.3% over 2400 cycles at 1 A g^{-1}	16
N-doped 1T MoS_2	3 m $Zn(CF_3SO_3)_2$	0.2–1.3 V	149.6 at 0.1 A g^{-1}	89.1% after 1000 cycles at 3 A g^{-1}	17
VS_2@N-C	3 m $Zn(CF_3SO_3)_2$	0.2–1.8 V	203 at 0.05 A g^{-1}	97% after 600 cycles at 1 A g^{-1}	18
Co-doped $Ni3Se_2$	1 m KOH and 0.25 m ZnO	1.4–1.9 V	179.34 at 1 A g^{-1}	85.9% after 1000 cycles at 1 A g^{-1}	19
MoS_2/Graphene	3 m $Zn(CF_3SO_3)_2$	0.2–1.5 V	283.9 at 0.1 A g^{-1}	88.6% after 1800 cycles at 1 A g^{-1}	3
MoS_2@CNTs	3 m $Zn(CF_3SO_3)_2$	0.3–1.2 V	161.5 at 0.1 A g^{-1}	80.1% after 500 cycles at 1 A g^{-1}	20
rGO-VS_2	3 m $Zn(CF_3SO_3)_2$	0.4–1.7 V	238 at 0.1 A g^{-1}	93% after 1000 cycles at 5.0 A g^{-1}	21
rGO-VSe_2	2 m $ZnSO_4$	0.2–1.4 V	221.5 at 0.5 A g^{-1}	91.6% after 150 cycles at 0.5 A g^{-1}	22
VS_4@rGO	1 m $Zn(CF_3SO_3)_2$	0–1.8 V	450 at 0.5 A g^{-1}	82% after 3500 cycles at 10 A g^{-1}	23
MoS3/MWCNTs	2 m $ZnSO_4$	0.01–2 V	368 at 0.5 A g-1	85.6% after 100 cycles at 0.5 A g^{-1}	24
MnS/RGO	2 m $ZnSO_4$ and 0.1 m $MnSO_4$	0.8–1.9 V	289 at 0.1 A g^{-1}	70.8% after 1000 cycles at 1 A g^{-1}	25
VS2@VOOH	3 m $Zn(CF_3SO3)_2$	0.4–1.0 V	165 at 0.1 A g^{-1}	86% after 200 cycles at 1.0 A g^{-1} [123]	26
VS2/VOx	25 m $ZnCl_2$	0.1–1.8 V	260 at 0.1 A g^{-1}	75% after 3000 cycles at 1.0 A g^{-1} [142]	27

References

1. Kresse, G. & Hafner, J. Ab initio molecular dynamics for liquid metals. *Phys. Rev. B* **47**, 558–561 (1993).

2. Henkelman, G., Uberuaga, B. P. & Jónsson, H. Climbing image nudged elastic band method for finding saddle points and minimum energy paths. *J. Chem. Phys.* **113**, 9901–9904 (2000).

3. Li, S. *et al.* Sandwich-Like Heterostructures of MoS2/Graphene with Enlarged Interlayer Spacing and Enhanced Hydrophilicity as High-Performance Cathodes for Aqueous Zinc-Ion Batteries. *Adv. Mater.* **33**, (2021).

4. Huang, M. *et al.* Tuning the kinetics of zinc ion in MoS2 by polyaniline intercalation. *Electrochim. Acta* **388**, (2021).

5. Liu, H. *et al.* Boosting zinc-ion intercalation in hydrated MoS2 nanosheets toward substantially improved performance. *Energy Storage Mater.* **35**, 731–738 (2021).

6. Zhang, Z. *et al.* Crystal water assisting MoS2 nanoflowers for reversible zinc storage. *J. Alloys Compd.* (2021) doi:10.1016/j.jallcom.2021.159599.

7. Liu, J. *et al.* Boosting aqueous zinc-ion storage in MoS2 via controllable phase. *Chem. Eng. J.* **389**, (2020).

8. Cai, C. *et al.* A nano interlayer spacing and rich defect 1T-MoS 2 as cathode for superior performance aqueous zinc-ion batteries . *Nanoscale Adv.* **3**, 3780–3787 (2021).

9. Liu, J. *et al.* Vertically aligned 1 T phase MoS2 nanosheet array for high-performance rechargeable aqueous Zn-ion batteries. *Chem. Eng. J.* **428**, (2022).

10. He, P. *et al.* Layered VS2 nanosheet-based aqueous Zn ion battery cathode. *Adv. Energy Mater.* **7**, 1601920 (2017).

11. Jiao, T. *et al.* Binder-free hierarchical VS2 electrodes for high-performance aqueous Zn ion batteries towards commercial level mass loading. *J. Mater. Chem. A* **7**, 16330–16338 (2019).

12. Tang, B. *et al.* Investigation of zinc storage capacity of WS2 nanosheets for rechargeable aqueous Zn-ion batteries. *J. Alloys Compd.* **894**, (2022).

13. Wen, L. *et al.* A novel TiSe2 (de)intercalation type anode for aqueous zinc-based energy storage. *Nano Energy* vol. 93 (2022).

14. Bai, Y. *et al.* Selenium Defect Boosted Electrochemical Performance of Binder-Free VSe2Nanosheets for Aqueous Zinc-Ion Batteries. *ACS Appl. Mater. Interfaces* **13**, 23230–23238 (2021).

15. Li, S. *et al.* Molecular Engineering on MoS2 Enables Large Interlayers and Unlocked Basal Planes for High-Performance Aqueous Zn-Ion Storage. *Angew. Chemie - Int. Ed.* **60**, 20286–20293 (2021).

16. Zhao, Y. *et al.* Vacancy Modulating Co3Sn2S2 Topological Semimetal for Aqueous Zinc-Ion Batteries. *Angew. Chemie - Int. Ed.* **61**, (2022).

17. Sheng, Z. *et al.* Nitrogen-Doped Metallic MoS2Derived from a Metal-Organic Framework for Aqueous Rechargeable Zinc-Ion Batteries. *ACS Appl. Mater. Interfaces* **13**, 34495–34506 (2021).

18. Liu, J., Peng, W., Li, Y., Zhang, F. & Fan, X. A VS2@N-doped carbon hybrid with strong interfacial interaction for high-performance rechargeable aqueous Zn-ion batteries. *J. Mater. Chem. C* **9**, 6308–6315 (2021).

19. Amaranatha Reddy, D. *et al.* Facile synthesis of cauliflower-like cobalt-doped Ni3Se2 nanostructures as high-performance cathode materials for aqueous zinc-ion batteries. *Int. J. Hydrogen Energy* **45**, 7741–7750 (2020).

20. Huang, M. *et al.* Hierarchical MoS2@CNTs Hybrid as a Long-Life and High-Rate Cathode for Aqueous Rechargeable Zn-Ion Batteries. *ChemElectroChem* **7**, 4218–4223 (2020).

21. Chen, T. *et al.* VS2 nanosheets vertically grown on graphene as high-performance cathodes for aqueous zinc-ion batteries. *J. Power Sources* **477**, (2020).

22. Narayanasamy, M. *et al.* Nanohybrid engineering of the vertically confined marigold structure of rGO-VSe2 as an advanced cathode material for aqueous zinc-ion battery. *J. Alloys Compd.* **882**, (2021).

23. Chen, K. *et al.* Robust VS4@rGO nanocomposite as a high-capacity and long-life cathode material for aqueous zinc-ion batteries. *Nanoscale* **13**, 12370–12378 (2021).

24. Liu, Y. *et al.* Performance and application of carbon composite MoS3 as cathode materials for aqueous zinc-ion batteries. *J. Alloys Compd.* **893**, (2022).

25. Ma, S. C. *et al.* In situ preparation of manganese sulfide on reduced graphene oxide sheets as cathode for rechargeable aqueous zinc-ion battery. *J. Solid State Chem.* **299**, (2021).

26. Pu, X. *et al.* Rose-like vanadium disulfide coated by hydrophilic hydroxyvanadium oxide with improved electrochemical performance as cathode material for aqueous zinc-ion batteries. *J. Power Sources* **437**, (2019).

27. Yu, D. *et al.* Boosting Zn2+ and NH4+ Storage in Aqueous Media via In-Situ Electrochemical Induced VS2/VOx Heterostructures. *Adv. Funct. Mater.* **31**, (2021).